Performance Analysis of OCDM for Wireless Communications

Muhammad Shahmeer Omar and Xiaoli Ma

***Abstract*—Orthogonal chirp division multiplexing (OCDM) was recently introduced as a new multi-carrier scheme based on the chirp spread spectrum (CSS) and shown to be more robust to interference caused by insufficient guard intervals. However, a thorough analysis of OCDM for wireless channels has not been conducted. Thus, this paper investigates the performance of OCDM affected by different impairments that are typical in a wireless channel and shows that uncoded OCDM performs better than OFDM and similar to single carrier block transmissions in multipath channels. Building on previous results, this study also shows that OCDM is more robust to time-burst interference (TBI) than its competitors and to narrow band interference (NBI) than OFDM because of spreading. However, OCDM is shown to suffer because of the loss of orthogonality caused by carrier frequency offset (CFO) and is analytically shown to have the same peak-to-average power ratio (PAPR) as OFDM.**

***Index Terms*—Orthogonal chirp division multiplexing (OCDM), OFDM, discrete Fresnel transform, narrow band interference, carrier frequency offset (CFO).**

I. Introduction

Fifth generation (5G) mobile networks are expected to cater to a plethora of different devices and use cases, each with its own set of requirements. There are three major classes of networks which fall under the umbrella of 5G, namely enhanced mobile broadband (eMBB), ultra reliable low latency communication (URLLC), and massive machine type communication (mMTC). Each class corresponds to a different use-case and has different requirements. For example, eMBB is required to deliver high data-rate uplink and downlink connections for mobile devices, URLLC needs to be reliable with latencies close to 1 ms, and mMTC needs to provide coverage to a large number of devices that operate with greater power efficiency and thus, have a longer network lifetime [1].

Orthogonal frequency division multiplexing (OFDM) has already been standardized as the modulation scheme to be employed for eMBB due to its high spectral efficiency and low complexity equalization. However, OFDM is known to be susceptible to burst errors that are caused by channel nulls or interference which significantly affect its average error performance. Due to these problems, it may not be able to guarantee the reliability constraints that are a feature of URLLC. Moreover, mMTC networks are bound to be interference limited due to operations in unlicensed bands. Hence, alternative schemes need to be investigated and spreading schemes, like orthogonal chirp division multiplexing (OCDM), show considerable promise when it comes to solving these problems.

OCDM has recently been introduced as a multi-carrier scheme for optical and wireless networks [2]–[8]. Based on the chirp spread spectrum (CSS) which has been used to provide secure, robust links for military applications and more recently in Long Range alliance (LoRa) networks for IoT applications, OCDM enables multiplexing chirps such that the maximum spectral efficiency can be achieved.

OCDM was first proposed in [2] and, through simulations, was shown to have better performance in linear time invariant (LTI) multipath channels than OFDM and greater resistance to interference caused by insufficient guard intervals. However, it was shown to have the same peak-to-average power ratio (PAPR) as OFDM. In [3], OCDM was applied to coherent optical-fiber communications and the performance was analyzed using several metrics such as bit error rate (BER), Q-factor, and PAPR. Double-sideband (DSB) modulated OCDM using intensity modulation was proposed in [4].

A block pilot-based channel estimation scheme was proposed for OCDM in [5], which made use of the root-Zadoff Chu sequence as the pilot and leveraged its relation to the discrete Fresnel transform (DFnT) to estimate the channel. In [6], OCDM was shown to perform better in multi-input multi-output (MIMO) systems with space-time coding than OFDM. A precoding scheme to enable orthogonal multiple user access and maximum diversity detection in frequency-selective channels for OCDM was proposed in [7] and spectral shaping techniques for OCDM were proposed in [8]. Orthogonal CSS was proposed in [9] which multiplexes an arbitrary number of continuous orthogonal chirps to asymptotically achieve the Nyquist signaling rate.

OCDM was analyzed for underwater acoustic (UWA) channels in [10], [11]. It was shown to be more resilient to time varying channels than OFDM as long as a subset of chirps is used in [10]. A rake receiver was designed in [11] to improve the performance of OCDM with large multipath and insufficient guard intervals. Real valued OCDM was designed for power line communications in [12] and was shown to perform better than OFDM and single carrier schemes. In [13], a low complexity iterative equalization technique, based on parallel interference cancellation (PIC), was designed for OCDM.

Although OCDM has started to gain more attention recently in different communication systems, the analysis of OCDM for different wireless channel impairments is still lacking. This paper analyzes the performance of OCDM for a variety of wireless channels and sets up performance base lines through comparisons with existing techniques such as OFDM and single carrier with frequency domain equalization (SC-FDE). With the aid of numerical simulations and, where possible,

M. S. Omar and X. Ma are with the School of Electrical and Computer Engineering, Georgia Institute of Technology, Atlanta, GA 30332, USA (emails: momar6@gatech.edu; xiaoli@gatech.edu).

This work is, in part, supported by an Industry/University Cooperative Research center of National Science Foundation Center on Fiber Wireless Integration and Networking (FiWIN) for heterogeneous mobile data communications under contract number 1539976.

The final version of record is available at http://dx.doi.org/10.1109/TWC.2021.3055070

mathematical analysis, this study thoroughly describes the performance of OCDM in LTI and linear time varying (LTV) channels, carrier frequency offset (CFO), and external interference that is limited in frequency or time, heretofore referred to as narrow band interference (NBI) and time-burst interference (TBI), respectively. Results for both coded and uncoded cases are presented and it is shown that not only does OCDM perform better than OFDM in multipath channels, it is also more robust to interference than other schemes.

In this work, upper case bold letters, such as $\mathbf{H}$ and lower case bold letters, such as $\mathbf{h}$ are used to represent matrices and vectors, respectively and $[\mathbf{A}]_{k,n} = A(k,n)$ denotes the element on the k^{th} row and n^{th} column of a matrix. The transpose and complex conjugate transpose of vectors and matrices are denoted by $(.)^T$ and $(.)^{\mathcal{H}}$, while $(.)^\star$ represents the element-wise conjugate. Diagonal matrices are represented by $\text{diag}(\mathbf{a})$ and $\text{diag}(a(k))$, where $\mathbf{a}$ and $a(k)$ are the vector and the k^{th} element on the main diagonal, respectively. The L_2 norm is denoted by $\|.\|$, expectation by $\mathbb{E}$, and matrix rank by $\mathcal{R}$. Modulo$-K$ operations are denoted by $(.)_K$

The remainder of this work is organized as follows: Section II introduces the system model, Section III presents equalization techniques for OCDM, Section IV analyzes the performance of OCDM in LTI channels, Section V presents the PAPR, Section VI discusses the impact of CFO, Section VII presents results for OCDM in LTV channels, Section VIII analyzes its performance in the presence of interference, and Section IX concludes the paper.

II. System Model

Consider OCDM transmissions where data bits are first encoded using forward error correction codes (FEC) and then mapped onto a complex alphabet. This study considers only quadrature phase shift keying (QPSK), keeping in mind that the impacts of using a higher order constellation have been well investigated. The resulting stream of symbols $u(n)$ is subsequently grouped into blocks of size N given by $\mathbf{u}(i) = [u(iN), u(iN+1), ..., u(iN+N-1)]^T$ and modulated using a set of orthogonal chirps, which can be implemented in the discrete domain using the IDFnT. The resulting block is given by $\mathbf{s}(i) = \mathbf{\Phi}^{\mathcal{H}}\mathbf{u}(i)$, where $\mathbf{\Phi}$ denotes an $N \times N$ DFnT matrix defined as

$$\Phi(m,n) = \frac{1}{\sqrt{N}} e^{-j\frac{\pi}{4}} \times \begin{cases} e^{j\frac{\pi}{N}(m-n)^2} & N \equiv 0 \text{ (mod 2)} \\ e^{j\frac{\pi}{N}(m+\frac{1}{2}-n)^2} & N \equiv 1 \text{ (mod 2).} \end{cases} \quad (1)$$

The DFnT matrix can be decomposed using the relation $\mathbf{\Phi} = \mathbf{\Theta}_2\mathbf{F}\mathbf{\Theta}_1$, where $\mathbf{\Theta}_1$ and $\mathbf{\Theta}_2$ are diagonal matrices given by

$$\Theta_1(m,m) = \begin{cases} e^{-j\frac{\pi}{4}} e^{j\frac{\pi}{N}m^2} & N \equiv 0 \text{ (mod 2)} \\ e^{-j\frac{\pi}{4}} e^{j\frac{\pi}{N}(m^2+m)} & N \equiv 1 \text{ (mod 2)}, \end{cases}$$

$$\Theta_2(n,n) = \begin{cases} e^{j\frac{\pi}{N}n^2} & N \equiv 0 \text{ (mod 2)} \\ e^{j\frac{\pi}{N}(n^2-n)} & N \equiv 1 \text{ (mod 2)}, \end{cases} \quad (2)$$

and $\mathbf{F}$ is the normalized discrete Fourier transform (DFT) matrix defined as $[\mathbf{F}]_{k,n} = \frac{1}{\sqrt{N}} e^{-j2\pi kn/N}$. Hence, the fast Fourier transform (FFT) algorithm can be leveraged for low complexity implementation. For simplicity, this paper only considers even values of N.

Dropping the block index and using the definition of the IDFnT in Eq. (1), the n^{th} element of the modulated symbol is given by

$$s(n) = e^{j\frac{\pi}{4}} \sum_{k=0}^{N-1} u(k) e^{-j\frac{\pi}{N}(n-k)^2}. \quad (3)$$

A cyclic prefix (CP) of length N_{g} is added and the resulting block is given by $\bar{\mathbf{s}} = \mathbf{T}_{\text{CP}}\mathbf{s}$, where $\mathbf{T}_{\text{CP}} = [\mathbf{I}_{\text{CP}}^T \ \mathbf{I}_{\text{N}}^T]^T$, with $\mathbf{I}_{\text{N}}$ and $\mathbf{I}_{\text{CP}}$ being the $N \times N$ identity matrix and the last N_{g} columns of $\mathbf{I}_{\text{N}}$, respectively. The resulting symbols are then serialized, passed through a pulse-shaping filter, up-converted and transmitted. Assuming a sampling rate of N/T_{s} Hz, where T_{s} is the symbol period (not including the CP), the interpolated continuous-time signal is given by

$$\bar{s}(t) = \begin{cases} s(t + T_{\text{s}} - T_{\text{g}}), & 0 \le t < T_{\text{g}} \\ s(t - T_{\text{g}}), & T_{\text{g}} \le t < T_{\text{s}} + T_{\text{g}} \end{cases} \quad (4)$$

where $T_{\text{g}} = N_{\text{g}}T_{\text{s}}/N$ is the CP duration. In order to define $s(t)$, we first introduce the continuous-time chirp as

$$\psi_0(t) = e^{j\frac{\pi}{4}} e^{-j\pi\frac{N}{T_{\text{s}}^2}t^2}, \quad 0 \le t < T_{\text{s}}.$$

It has been shown in [2], that interpolating the discrete samples results in the periodically extended continuous time signal, given by

$$s(t) = \sum_{k=0}^{N-1} u(k)\tilde{\psi}_k(t)\Pi_{T_{\text{s}}}(t) = \sum_{k=0}^{N-1} u(k)\tilde{\psi}_0\left(t - \frac{kT_{\text{s}}}{N}\right)\Pi_T(t), \quad (5)$$

where $\Pi_T(t) = 1$ if $0 \le t < T_{\text{s}}$ and 0 otherwise, and the root chirp $\tilde{\psi}_0$ is given by

$$\tilde{\psi}_0(t) = \begin{cases} e^{j\frac{\pi}{4}} e^{-j\pi\frac{N}{T_{\text{s}}^2}t^2}, & \text{if } -\frac{T_{\text{s}}}{2} \le t < \frac{T_{\text{s}}}{2}, \\ e^{j\frac{\pi}{4}} e^{-j\pi\frac{N}{T_{\text{s}}^2}(t-cT_{\text{s}})^2}, & \text{if } -\frac{T_{\text{s}}}{2} + cT_{\text{s}} \le t < \frac{T_{\text{s}}}{2} + cT_{\text{s}}. \end{cases} \quad (6)$$

Owing to the periodicity property, sampling the interpolated signal recovers the discrete symbol defined in Eq. (3).

At the receiver, the signal is down-converted to the baseband using a local oscillator, which may not be completely synchronized with the transmitter, and passed through a receive filter to give

$$y(t) = e^{j2\pi\Delta_f t} \int h(t;\tau)\bar{s}(t-\tau)d\tau + v(t), \quad (7)$$

where $h(t,\tau)$ models the aggregate effect of the channel and the transmit and receive filters, τ denotes the tap delay, Δ_f denotes the CFO which occurs due to oscillator mismatch or phase noise, and $v(t)$ represents additive white Gaussian noise (AWGN). We model the channel as a finite impulse response (FIR) filter with a maximum delay spread of LT_{s}/N. Thus, the discrete-time baseband signal, obtained by sampling $y(t)$ is given by

$$y(n) = y(t)\big|_{t=\frac{nT_{\text{s}}}{N}} = e^{j2\pi\frac{\Delta_f T_{\text{s}}}{N}n} \sum_{l=0}^{L} h(n;l)\bar{s}(n-l) + v(n). \quad (8)$$

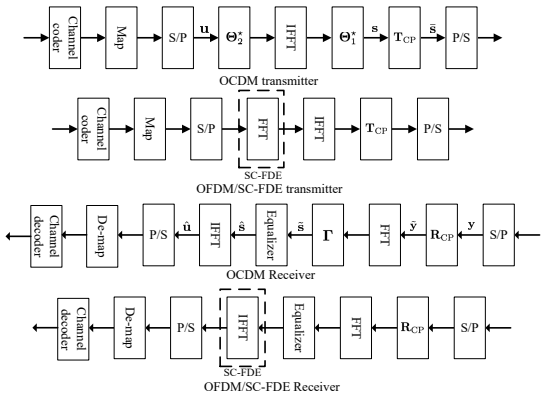

Fig. 1. Block diagrams for OCDM, OFDM and SC-FDE baseband transmitters and receivers.

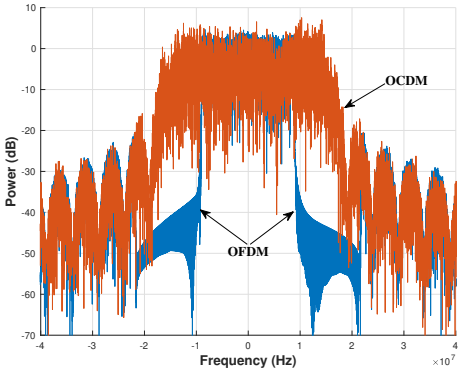

Fig. 2. Spectral characteristics of OCDM and OFDM.

For the remainder of this paper, we assume that $N_{\rm g} = L$ and thus, there is no inter-block interference (IBI). Making the substitution $\epsilon = \Delta_f T_{\rm s}$, the matrix-vector form of Eq. (8) is

$$\mathbf{y}(i) = e^{\frac{j2\pi\epsilon P}{N} i} \tilde{\mathbf{D}}_f (\bar{\mathbf{H}}_0(i)\bar{\mathbf{s}}(i) + \bar{\mathbf{H}}_1(i)\bar{\mathbf{s}}(i-1)) + \mathbf{v}(i) \quad (9)$$

where the $P \times P$ matrices $[\bar{\mathbf{H}}_0(i)]_{n,l} = h(iP+n; n-l)$ and $[\bar{\mathbf{H}}_1(i)]_{n,l} = h(iP+n; P+n-l)$ are the channel matrices, $P = N + L$ and $h(n;l) = 0\ \forall l > L$. The $P \times P$ diagonal matrix $\tilde{\mathbf{D}}_f$ is given by $\text{diag}(e^{j2\pi\epsilon(n-1)/N})$, $n \in [1, P]$.

The first step at the receiver, after serial-to-parallel conversion (S/P), is to remove the CP which can be represented by the operation $\tilde{\mathbf{y}}(i) = \mathbf{R}_{\rm CP}\mathbf{y}(i)$, where $\mathbf{R}_{\rm CP} = [\mathbf{0}_{N\times L}\ \mathbf{I}_N]$. Hence, the received symbol is given by

$$\begin{aligned}\tilde{\mathbf{y}}(i) &= e^{\frac{j2\pi\epsilon P}{N} i}\mathbf{R}_{\rm CP}(\tilde{\mathbf{D}}_f\bar{\mathbf{H}}_0(i)\bar{\mathbf{s}}(i) + \bar{\mathbf{H}}_1(i)\bar{\mathbf{s}}(i-1) + \mathbf{R}_{\rm CP}\mathbf{v}(i) \\ &= e^{\frac{j2\pi\epsilon(iP+L)}{N}}\mathbf{D}_f\mathbf{H}(i)\mathbf{\Phi}^{\mathcal{H}}\mathbf{u}(i) + \tilde{\mathbf{v}}(i), \end{aligned} \quad (10)$$

where the equality follows from $\mathbf{R}_{\rm CP}\tilde{\mathbf{D}}_f = e^{\frac{j2\pi\epsilon L}{N}}\mathbf{D}_f\mathbf{R}_{\rm CP}$ and $\mathbf{D}_f = \text{diag}(e^{j2\pi\epsilon(n-1)/N})$ is an $N \times N$ matrix, as shown in [14], [15]. Furthermore, when $N_{\rm g} \geq L$, $\mathbf{R}_{\rm CP}\bar{\mathbf{H}}_1(i) = \mathbf{0}_{N\times P}$ and $\mathbf{H}(i) = \mathbf{R}_{\rm CP}\bar{\mathbf{H}}_0(i)\mathbf{T}_{\rm CP}$, where $[\mathbf{H}(i)]_{n,l} = h(iP+L+n; (n-l)_N)$. The resulting signal is equalized, demapped and decoded as shown in Fig. 1. For comparison, the transceiver structures for OFDM and SC-FDE are also shown.

Fig. 2 plots the spectra of the OCDM and OFDM signals when only a subset of channels is used for transmission. We assume a sampling rate of 30.72 MHz, FFT size of $N = 2,048$, with $N_{\rm g} = N/8$, an oversampling rate of 4 and root-raised-cosine pulse shaping. Since, OCDM spreads each symbol over the entire band, reducing the number of active sub-channels does not have any impact on its spectrum. On the other hand, the bandwidth of OFDM is directly affected by the number of active subcarriers, a fact that is often used to meet spectral mask requirements.

III. Equalization of OCDM

Consider OCDM transmissions with perfect synchronization, i.e., $\epsilon = 0$. In this case, Eq. (10) is simplified as

$$\tilde{\mathbf{y}} = \mathbf{H}\mathbf{\Phi}^{\mathcal{H}}\mathbf{u} + \tilde{\mathbf{v}}, \quad (11)$$

where the block index i has been dropped for brevity. While OCDM can be equalized in both the time and frequency domains, we primarily focus on frequency domain equalization (FDE) owing to its lower complexity when the channel is LTI. We assume time domain equalization (TDE) only when considering maximum likelihood equalization (MLE) for LTI channels.

In TDE, the received signal is first equalized in the time domain before being converted to the Fresnel domain by computing the DFnT. However, in LTI channels, the matrix $\mathbf{H}$ in Eq. (11) becomes an $N \times N$ circulant matrix whose first column is given by $[h(0), h(1), ..., h(L), 0, ..., 0]^T$, where $h(n)$, $n \in [0, L]$ are assumed to be zero-mean complex Gaussian random variables. Due to the circular convolution property of the DFnT, the order of operations can be reversed, i.e., the DFnT can be computed first. The resulting block is given by

$$\hat{\mathbf{y}} = \mathbf{\Phi}\tilde{\mathbf{y}} = \mathbf{\Phi}\mathbf{H}\mathbf{\Phi}^{\mathcal{H}}\mathbf{u} + \mathbf{\Phi}\tilde{\mathbf{v}} = \mathbf{H}\mathbf{u} + \mathbf{\Phi}\tilde{\mathbf{v}}, \quad (12)$$

which can then be equalized using MLE.

Since $\mathbf{\Phi}$ is circulant [2], [3], it can be diagonalized by the DFT such that $\mathbf{\Phi} = \mathbf{F}^{\mathcal{H}}\mathbf{\Gamma}\mathbf{F}$, where $\mathbf{\Gamma} = \text{diag}(e^{-j\frac{\pi}{N}k^2})$ $\forall k \in [0, N-1]$. By making this substitution, Eq. (11) can be reformulated as

$$\tilde{\mathbf{y}} = \mathbf{H}\mathbf{F}^{\mathcal{H}}\mathbf{\Gamma}^{\mathcal{H}}\mathbf{F}\mathbf{u} + \tilde{\mathbf{v}}. \quad (13)$$

After computing the DFT of the received signal, we get

$$\bar{\mathbf{y}} = \mathbf{F}\tilde{\mathbf{y}} = \mathbf{H}_f\mathbf{\Gamma}^{\mathcal{H}}\mathbf{F}\mathbf{u} + \mathbf{F}\tilde{\mathbf{v}}, \quad (14)$$

where $\mathbf{H}_f = \mathbf{F}\mathbf{H}\mathbf{F}^{\mathcal{H}}$ is an $N \times N$ frequency domain channel matrix. The zero-forcing (ZF) and minimum mean squared error (MMSE) equalizers for OCDM can then be defined as

$$\mathbf{G}_{\rm ZF} = \mathbf{F}^{\mathcal{H}}\mathbf{\Gamma}(\mathbf{H}_f^{\mathcal{H}}\mathbf{H}_f)^{-1}\mathbf{H}_f^{\mathcal{H}}, \quad (15)$$

and

$$\mathbf{G}_{\rm MMSE} = \mathbf{F}^{\mathcal{H}}\mathbf{\Gamma}\mathbf{H}_f^{\mathcal{H}}\left(\mathbf{H}_f\mathbf{H}_f^{\mathcal{H}} + \frac{\mathcal{N}_0}{E_s}\mathbf{I}_N\right)^{-1}, \quad (16)$$

where E_s and $\mathcal{N}_0$ are the symbol and noise variances, respectively.

A special case of Eq. (14) occurs when the channel is LTI. In this case the frequency domain channel matrix becomes a diagonal matrix, i.e., $\mathbf{H}_f = \mathbf{D}_h = \text{diag}([H(0), H(1), ..., H(N-1)])$, where $H(k)$ is the channel frequency response (CFR) at

the k^{th} frequency component. Now we can apply the phase rotation to received block in Eq. (14) to result in the symbols given by

$$\tilde{\mathbf{s}} = \mathbf{\Gamma}\bar{\mathbf{y}} = \mathbf{D}_h\mathbf{F}\mathbf{u} + \mathbf{\Gamma}\mathbf{F}\tilde{\mathbf{v}}. \tag{17}$$

In this case, the linear equalizers defined in Eq. (15) and Eq. (16) become single tap equalizers that can be denoted by diagonal matrices whose k^{th} diagonal element is given by $\frac{1}{H(k)}$ and $\frac{H^\star(k)}{|H(k)|^2+\mathcal{N}_0/E_s}$, respectively.

Remark (similarities between OCDM and SC-FDE): Consider the OCDM signal given by Eq. (14) and compare with the equivalent signal for SC-FDE, which is given by $\bar{\mathbf{y}} = \mathbf{H}_f\mathbf{F}\mathbf{u}+\mathbf{F}\tilde{\mathbf{v}}$. Since $\mathbf{H}_f$ is the same for both schemes, the only difference is the term $\mathbf{\Gamma}^{\mathcal{H}}$. Hence, the equalizers for SC-FDE can be defined by simply removing $\mathbf{\Gamma}$ from Eq. (15) and Eq. (16). Since $\mathbf{\Gamma}$ is diagonal and unitary, it has no impact on the symbol and noise statistics. Compared with Eq. (14), under the same channel, OCDM and SC-FDE may exhibit the same performance. We will verify this using numerical simulations in subsequent sections.

IV. Performance in LTI Channels

A. Multipath diversity in uncoded OCDM

Multipath diversity is defined as the gradient of the logarithm of the error probability and the SNR and is given by

$$G_{d,e} = \lim_{E_b/N_0\to\infty} -\frac{\log \mathcal{P}_b}{\log(E_b/\mathcal{N}_0)}, \tag{18}$$

where $\mathcal{P}_b$ is the bit error probability, and E_b is the average energy per bit. Consider the received symbols in the Fresnel domain given by Eq. (12). Define $\mathbf{h} = [h(0), h(1), ..., h(L)]^T$. The conditional pair-wise error probability (PEP) is upper bounded by (c.f. [16], [17])

$$P(\mathbf{u}\to\mathbf{u}'|\mathbf{h}) \le \exp\left[-\frac{d^2(\hat{\mathbf{y}}',\hat{\mathbf{y}})}{4N_0}\right], \tag{19}$$

where $d^2(\hat{\mathbf{y}}',\hat{\mathbf{y}}) = \|\hat{\mathbf{y}}'-\hat{\mathbf{y}}\|^2$. Using the definition of $\hat{\mathbf{y}}$, we get

$$\begin{aligned}\|\hat{\mathbf{y}}'-\hat{\mathbf{y}}\|^2 &= \|\mathbf{H}(\mathbf{u}'-\mathbf{u})\|^2 \\ &= \|\mathbf{F}^{\mathcal{H}}\mathbf{D}_h\mathbf{F}(\mathbf{u}'-\mathbf{u})\|^2.\end{aligned}$$

Substituting $\mathbf{e} = \mathbf{F}(\mathbf{u}'-\mathbf{u})$ and noting that $\mathbf{F}^{\mathcal{H}}$ is a unitary matrix, we get $d^2(\hat{\mathbf{y}}',\hat{\mathbf{y}}) = \|\mathbf{D}_h\mathbf{e}\|^2 = \|\mathbf{D}_e\tilde{\mathbf{h}}\|^2$, where $\mathbf{D}_e = \text{diag}(\mathbf{e})$ and $\tilde{\mathbf{h}} = [H(0), H(1), ..., H(N-1)]^T$ is a column vector containing the CFR. Defining $\mathbf{W}$ as the truncated $N\times(L+1)$ DFT matrix, $\mathbf{R}_h = \mathbf{B}\mathbf{B}^{\mathcal{H}}$ as the positive definite auto-correlation matrix of $\mathbf{h}$, and making the substitutions $\tilde{\mathbf{h}} = \mathbf{W}\mathbf{B}\bar{\mathbf{h}}$, where $\bar{\mathbf{h}}$ is a length-$(L+1)$ column vector of independent and identically distributed (i.i.d.) zero-mean complex normal random variables, we get

$$d^2(\hat{\mathbf{y}}',\hat{\mathbf{y}}) = \|\mathbf{D}_e\tilde{\mathbf{h}}\|^2 = \bar{\mathbf{h}}^{\mathcal{H}}\mathbf{C}_e\bar{\mathbf{h}}, \tag{20}$$

where $\mathbf{C}_e = \mathbf{B}^{\mathcal{H}}\mathbf{W}^{\mathcal{H}}\mathbf{D}_e^{\mathcal{H}}\mathbf{D}_e\mathbf{W}\mathbf{B}$. We know that $G_{d,e} = \mathcal{R}(\mathbf{C}_e)$ and considering that $\mathbf{R}_h$, $\mathbf{B}$ are full rank and $\mathbf{C}_e$ is an $(L+1)\times(L+1)$ matrix, the maximum achievable diversity gain is $L+1$, given that $N \ge L+1$. However, $\mathbf{D}_e$ is not guaranteed to be full rank. In fact, $\mathcal{R}(\mathbf{D}_e)$ depends on the number of non-zero entries in $\mathbf{e}$ which in turn depends on the symbol vector $\mathbf{u}$. This is also the case for SC-FDE, as shown in [16]. In fact, the matrix $\mathbf{C}_e$ is identical for OCDM and SC-FDE, hence it follows that the performance should be the same. For very large SNR, the rank-1 errors, i.e. when $\mathcal{R}(\mathbf{D}_e) = 1$, dominate and OCDM (and SC-FDE) collect unit diversity.

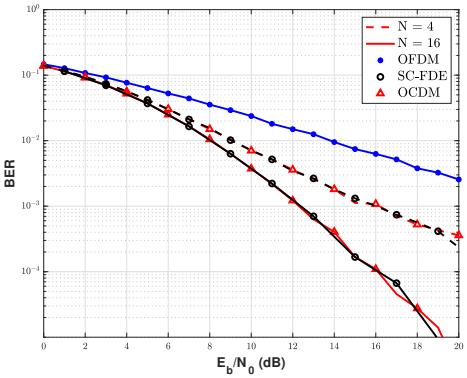

Fig. 3. Performance of OCDM with MLE for different N and $L = 2$.

Fig. 3 compares the performance of uncoded OCDM, SC-FDE, and OFDM using MLE. It can be seen that SC-FDE and OCDM show identical performance for different block sizes and both perform significantly better than uncoded OFDM. Each symbol in OFDM is detected independently, owing to the independence of the frequency subcarriers. As a result, uncoded OFDM can only collect unit diversity regardless of block size. On the other hand, OCDM and SC-FDE transmissions exhibit a diversity order greater than one which implies that the operating SNR is less than the threshold derived in [16] and the rank-1 errors are not yet dominant. Furthermore, the performance is dependent on the block size with larger blocks resulting in greater diversity. Considering that the diversity is dependent on $\mathcal{R}(\mathbf{D}_e)$, there are only a finite number of permutations of $\mathbf{u}$ where $\mathcal{R}(\mathbf{D}_e) = 1$. The probability of these permutations decreases with increasing N thus larger block sizes show better performance.

B. Uncoded performance with linear and decision feedback equalization

Consider the frequency domain symbols given by Eq. (17). It is easy to see that using a general equalizer $\mathbf{G} \in \{\mathbf{G}_{\text{ZF}}, \mathbf{G}_{\text{MMSE}}\}$ and converting the symbols back to the time domain results in the block given by

$$\hat{\mathbf{u}} = \mathbf{F}^{\mathcal{H}}\mathbf{G}\mathbf{D}_h\mathbf{F}\mathbf{u} + \mathbf{F}^{\mathcal{H}}\mathbf{G}\mathbf{\Gamma}\mathbf{F}\tilde{\mathbf{v}}. \tag{21}$$

We know that the BER for QPSK is given by (c.f. [19]–[21]),

$$\mathcal{P}_b = \frac{1}{N}\sum_{l=0}^{N-1} Q(\sqrt{\bar{\gamma}(l)}), \tag{22}$$

where $\bar{\gamma}(l)$ is the output signal-to-interference-and-noise ratio (SINR) on the l^{th} sub-channel, and $Q(r) = \frac{1}{\sqrt{2\pi}}\int_r^\infty e^{-t^2/2}dt$, $r \ge 0$. Hence, we use the output SINR to analyze the performance of OCDM with linear equalization. Looking at

the l^{th} element of the vector $\hat{\mathbf{u}}$ in Eq. (21) and substituting the value of the ZF equalizer taps, we get

$$\hat{u}(l) = u(l) + \frac{1}{N}\sum_{k=0}^{N-1}\frac{1}{H(k)}e^{-j\frac{\pi}{n}k^2}\sum_{n=0}^{N-1}\tilde{v}(n)e^{-j\frac{2\pi}{N}nk}e^{j\frac{2\pi}{N}lk}. \tag{23}$$

It is then fairly easy to see that the MSE on the l^{th} sub-channel is given by

$$\sigma^2(l) = \mathbb{E}\{|\hat{u}(l) - u(l)|^2\} = \frac{\mathcal{N}_0}{N}\sum_{k=0}^{N-1}\frac{1}{|H(k)|^2}. \tag{24}$$

Thus, combining Eqs. (23) and (24), we get

$$\bar{\gamma}(l) = \frac{E_s}{\sigma^2(l)} = \frac{\gamma}{\frac{1}{N}\sum_{k=0}^{N-1}\frac{1}{|H(k)|^2}}, \tag{25}$$

where $\gamma = E_s/\mathcal{N}_0$. It is pertinent to note that σ^2, and hence $\bar{\gamma}$, is independent of the sub-channel index l. Hence, it can be concluded that the noise is evenly distributed to all chirps in OCDM when ZF equalization is used.

In contrast with ZF equalizers, MMSE equalizers do not eliminate ISI but rather leverage it to avoid noise enhancement. After substituting the value of the MMSE equalizer taps into Eq. (21), the l^{th} element of the vector $\hat{\mathbf{u}}$ is given by

$$\hat{u}(l) = \frac{1}{N}\sum_{k=0}^{N-1}\sum_{n=0}^{N-1}\frac{|H(k)|^2}{|H(k)|^2+1/\gamma}u(n)e^{-j\frac{2\pi}{N}nk}e^{j\frac{2\pi}{N}lk} + \frac{1}{N}\sum_{k=0}^{N-1}\sum_{n=0}^{N-1}\frac{H^\star(k)}{|H(k)|^2+1/\gamma}\tilde{v}(n)e^{-j\frac{2\pi}{N}nk}e^{j\frac{2\pi}{N}lk}e^{-j\frac{\pi}{n}k^2}.$$

Decomposing the expression into the desired component and interference results in

$$\hat{u}(l) = \overbrace{\frac{1}{N}\sum_{k=0}^{N-1}\frac{|H(k)|^2}{|H(k)|^2+1/\gamma}}^{a}u(l) + \frac{1}{N}\sum_{k=0}^{N-1}\frac{|H(k)|^2}{|H(k)|^2+1/\gamma}\times \sum_{\substack{n=0\\n\neq l}}^{N-1}u(n)e^{-j\frac{2\pi}{N}nk}e^{j\frac{2\pi}{N}lk} + \frac{1}{N}\sum_{k=0}^{N-1}\frac{H^\star(k)}{|H(k)|^2+1/\gamma}e^{-j\frac{\pi}{n}k^2}\times \sum_{n=0}^{N-1}\tilde{v}(n)e^{-j\frac{2\pi}{N}nk}e^{j\frac{2\pi}{N}lk}, \tag{26}$$

which can be simplified to the form $\hat{u}(l) = au(l)+\tau(l)$, where $\tau(l)$ denotes the combined effect of the noise and interference. Hence, the output SINR is given by

$$\bar{\gamma}(l) = \frac{\mathbb{E}\{|au(l)|^2\}}{\mathbb{E}\{|\tau(l)|^2\}} = \frac{E_s|a|^2}{\mathbb{E}\{|\tau(l)|^2\}}. \tag{27}$$

Assuming that the input symbols are i.i.d. and that the noise and symbols are independent, it is easy to see that

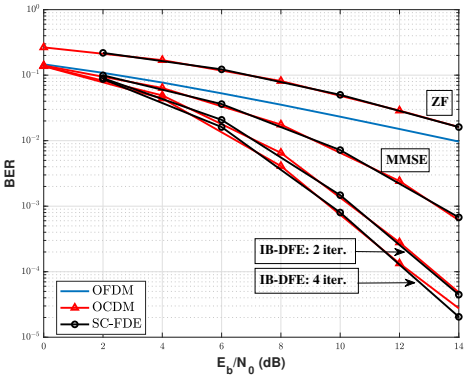

Fig. 4. Performance comparison of LE and IB-DFE for OCDM, SC-FDE and OFDM where $N = 64$ and $L = 8$.

$\mathbb{E}\{|\tau(l)|^2\} = \mathbb{E}\{|\hat{u}(l)|^2\} - |a|^2E_s$ and

$$\mathbb{E}\{|\hat{u}(l)|^2\} = \frac{1}{N}\sum_{k=0}^{N-1}\frac{|H(k)|^4}{(|H(k)|^2+1/\gamma)^2}E_s + \frac{\mathcal{N}_0}{N}\sum_{k=0}^{N-1}\frac{|H(k)|^2}{(|H(k)|^2+1/\gamma)^2} = \frac{E_s}{N}\sum_{k=0}^{N-1}\frac{|H(k)|^2}{|H(k)|^2+1/\gamma}, \tag{28}$$

where the equality follows from substituting $\gamma = E_s/\mathcal{N}_0$. Thus, it can be seen that $\mathbb{E}\{|\hat{u}(l)|^2\} = aE_s$. Substituting into the expression for the interference variance, we get $\mathbb{E}\{|\tau(l)|^2\} = aE_s - a^2E_s$. Hence, the output SINR is given by (c.f. Eq. (26))

$$\bar{\gamma}(l) = \frac{a^2E_s}{aE_s - a^2E_s} = \frac{\left(\sum_{k=0}^{N-1}\frac{|H(k)|^2}{|H(k)|^2+1/\gamma}\right)}{\left(\sum_{k=0}^{N-1}\frac{1}{\gamma|H(k)|^2+1}\right)}. \tag{29}$$

Again, we see that $\bar{\gamma}$ is independent of the sub-channel index. Hence all chirps have the same SINR. This behavior is the opposite of uncoded OFDM, where each sub-channel is independent and hence experiences different SINR depending on the CFR. It is also pertinent to note that the expressions for SINR shown in Eqs. (25) and (29) are identical to those derived for SC-FDE systems in [19]. Hence, it follows that OCDM and SC-FDE should have the same average BER performance.

We resort to numerical simulations to analyze the performance of OCDM with IB-DFE employing soft decisions. Fig. 4 compares the performance of the considered schemes with linear and decision feedback equalization. We can see that OCDM and SC-FDE perform identically for both LEs, which follows from the fact that the output SINR for OCDM and SC-FDE are the same. OCDM with MMSE equalization performs significantly better than OFDM and shows a 5 dB gain when BER is 10^{-2}. However, OCDM with ZF equalization shows worse performance than OFDM at lower SNRs and the BER seems to converge with OFDM as the SNR increases. This is a direct consequence of the noise amplification problem inherent in ZF equalizers. OCDM and SC-FDE also show

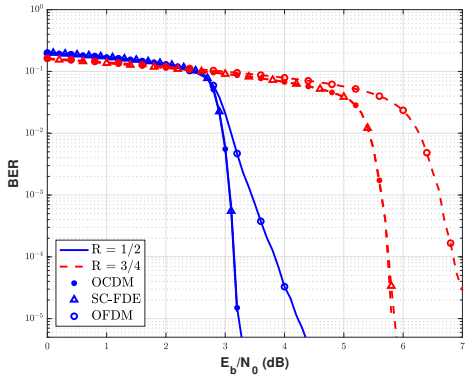

Fig. 5. BER performance of LDPC codes with the different transmission formats.

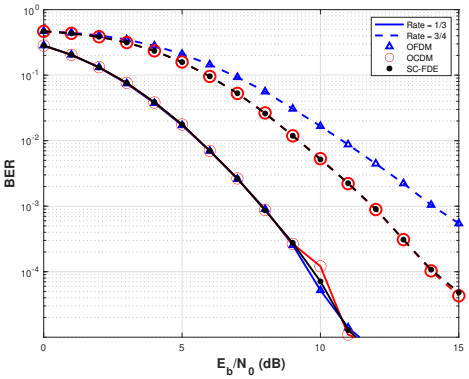

Fig. 7. BER performance with CC.

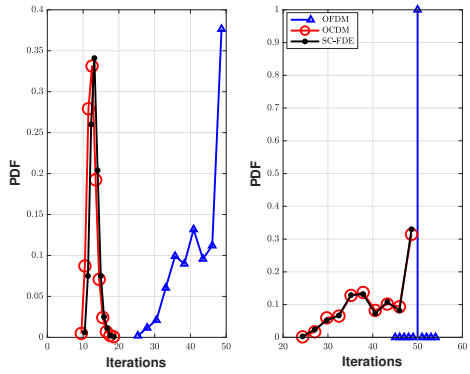

Fig. 6. Empirical probability density function (PDF) of the number of iterations required to satisfy the parity checks for rate $1/2$ codes when (left) SNR = 4.5 dB and (right) SNR = 3 dB

identical performance with IB-DFE because of the similarities in the transmission formats in the given conditions which were highlighted in Section III.

C. Coded OCDM

In this section, we compare the performance of OFDM, OCDM, and SC-FDE with two different channel codes using simulations: convolutional codes (CC) and low density parity check (LDPC) codes. We assume separate equalization (MMSE) and decoding.

Fig. 5 compares the performance of the three transmission formats when LDPC codes are employed. In this simulation the sampling rate is assumed to be 30.72 MHz, $N = 2,048$ with all sub-channels carrying data, the average symbol energy is normalized by the code rate and the codeword length is $64,800$. The channel is quasi-static and follows the EVA channel model [22], with tap delays and relative powers listed in Table I. In coded transmissions, the performance gap between OFDM and OCDM/SC-FDE is significantly reduced while OCDM and SC-FDE still perform identically. This is because coding enables OFDM to collect multipath diversity, which is not the case when there is no channel coding. Because channel changes every symbol and the codeword spans multiple symbols, the performance of all three schemes is significantly better due to both time and multipath diversity.

TABLE I
EVA CHANNEL MODEL

Excess tap delay (ns)	0	30	150	310	370	710	1090	1730	2510
Relative power (dB)	0	-1.5	-1.4	-3.6	-0.6	-9.1	-7.0	-12.0	-16.9

Fig. 6 plots the empirical probability densities of the number of iterations required for the LDPC decoder to converge. The maximum number of iterations has been set to 50. It can be seen that when SNR is 4.5 dB, SC-FDE and OCDM require a significantly lower number of iterations to satisfy the parity checks. The number of iterations are clustered around a mean of around 12-13 iterations. In contrast, the algorithm requires a greater number of iterations when OFDM is used. In fact, the decoder runs for all 50 iterations approximately 38% of the time for OFDM which explains why the BER is higher. Since, the equalizer and decoder are separate, the decoder uses the log-likelihood ratios (LLR) at the output of the equalizer and subsequent decision device. Hence, the decoding performance relies heavily on the equalizers ability to recover the constellation. As shown previously, the MMSE equalizer for SC-FDE and OCDM performs significantly better than OFDM, and thus the decoder is able to converge faster. The same thing occurs when the SNR is reduced to 3 dB. In this case the decoder requires the maximum number of iterations to decode every codeword when OFDM is employed.

Fig. 7 compares the performance of the three transmission formats when CC is used. We employ a rate-$1/3$ code with a constraint length of 7. Higher rate codes are obtained through puncturing and the codewords are block interleaved prior to modulation. Unlike the previous result, we fix the codeword length to fit within one symbol. A soft Viterbi decoder is employed at the receiver. At a code rate of $1/3$, we see that all three schemes perform the same. This is primarily because coded OFDM is able to collect multipath diversity whereas uncoded OFDM cannot. However, when the code rate of $3/4$ is used, OCDM and SC-FDE both perform better than OFDM because of better equalizer performance. For example, at BER

The final version of record is available at http://dx.doi.org/10.1109/TWC.2021.3055070

of 10^{-3}, OCDM and SC-FDE have an approximately 2 dB advantage over OFDM.

V. Peak-to-Average Power Ratio

In this section, we build on the simulation-based PAPR analysis of OCDM in [2], [3] and present an analytical expression for the PAPR distribution of OCDM. Ignoring the CP, the instantaneous PAPR is defined by

$$\text{PAPR}_i = \frac{\|\mathbf{s}(i)\|_\infty^2}{\mathbb{E}\{\|\mathbf{s}\|^2\}/(N)}, \tag{30}$$

which is a random variable since the input symbols are random. Hence, we use the complementary cumulative distribution function (CCDF), given by $\mathbb{P}(\text{PAPR}_i > T)$, as the measure in our analysis.

Assuming the input symbols are zero mean, i.i.d. random variables with independent in-phase and quadrature components, the real and imaginary parts of the n^{th} element an OCDM block are given by

$$Re(s(n)) = \frac{1}{\sqrt{N}} \sum_{k=0}^{N-1} X^{(n)}(k) + Y^{(n)}(k)$$
$$Im(s(n)) = \frac{1}{\sqrt{N}} \sum_{k=0}^{N-1} W^{(n)}(k) - Z^{(n)}(k),$$

where $X^{(n)}(k) = Re(u(k))\cos(\frac{\pi}{N}(k-n)^2 + \frac{\pi}{4})$, $Y^{(n)}(k) = Im(u(n))\sin(\frac{\pi}{N}(k-n)^2 + \frac{\pi}{4})$, $W^{(n)}(k) = Im(u(n))\cos(\frac{\pi}{N}(k-n)^2 + \frac{\pi}{4})$ and $Z^{(n)}(k) = Re(u(n))\sin(\frac{\pi}{N}(k-n)^2 + \frac{\pi}{4})$. Using these, we see that

$$\mathbb{E}\{Re(s(n))Im(s(m))\} = \mathbb{E}\Bigg\{\left(\frac{1}{\sqrt{N}}\sum_{n=0}^{N-1} X^{(n)}(k) + Y^{(n)}(k)\right) \times \left(\frac{1}{\sqrt{N}}\sum_{n=0}^{N-1} W^{(m)}(k) - Y^{(m)}(k)\right)\Bigg\}$$
$$\overset{(a)}{=} \frac{1}{N}\sum_{n=0}^{N-1}\left(\mathbb{E}\{(X^{(n)}(k) + Y^{(n)}(k))(W^{(m)}(k) - Y^{(m)}(k)\}\right)$$
$$\overset{(b)}{=} \frac{E_s}{2N}\sum_{n=0}^{N-1}\sin\left(\frac{2\pi n}{N}(m-n) + \frac{\pi}{N}(n^2-m^2)\right)$$
$$= 0,$$

where (a) follows from the independence of the symbols and (b) is obtained by substituting the values of $X^{(n)}(k), Y^{(n)}(k), W^{(n)}(k), Z^{(n)}(k)$ and using the fact that the symbols have independent real and imaginary parts. Through similar reasoning and using the above result, it is straight forward to show that $\mathbb{E}\{\mathbf{s}\mathbf{s}^{\mathcal{H}}\} = E_s\mathbf{I}_N$.

Having established that $s(n)$'s are i.i.d. random variables with zero mean, we can use the Lyapunov central limit theorem to show that as $N \to \infty$, the OCDM symbols can be approximated by i.i.d. normal random variables, as it has been shown in [23]. Hence the CCDF of the PAPR of OCDM is given by

$$\mathbb{P}(\text{PAPR}_i > \text{T}) = 1 - [1 - e^{-\text{T}}]^N, \tag{31}$$

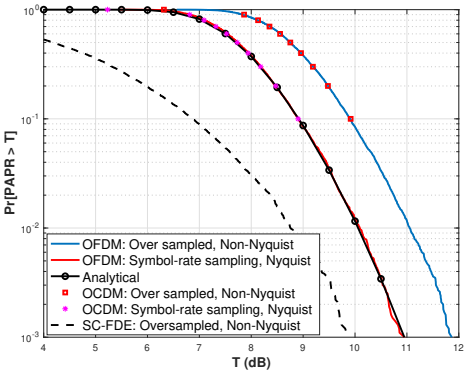

Fig. 8. CCDF of PAPR for OCDM, OFDM and SC-FDE with $N = 256$ and $N_{\text{CP}} = 16$.

which is identical to that of OFDM.

Fig. 8 compares the PAPR of OCDM and OFDM symbols using the CCDF as the metric for comparison. The PAPR has been measured for two cases using simulations, namely with symbol rate sampling and Nyquist pulse shaping and with signals over sampled at four times of the symbol rate with the root raised cosine filter used as the pulse shaping filter. For reference, the PAPR of the over sampled, non-Nyquist pulse shaped SC-FDE signal has also been shown. The graph shows that OFDM and OCDM have identical performance, and are closely approximated by Eq. (31) when considering the symbol rate sampling scenario. Moreover, we see that the PAPR is greater by 1-2 dB when non-Nyquist pulse shapes are used owing to the ISI. However, the PAPR of SC-FDE is considerably lower. In fact at probability of 10^{-3}, SC-FDE shows a 2 dB lower PAPR than both OFDM and OCDM.

VI. Carrier Frequency Offset

In this section, we examine the impacts of CFO on OCDM transmissions. We assume an LTI frequency selective channel. Consider the discrete symbols given by Eq. (10). Taking the DFT at the receiver and multiplying with $\mathbf{\Gamma}$, we get

$$\tilde{\mathbf{s}}(i) = \mathbf{\Gamma}\mathbf{F}\tilde{\mathbf{y}}(i) = e^{\frac{j2\pi\epsilon(iP+L)}{N}} e^{j\pi\frac{\epsilon(N-1)}{N}} \mathbf{\Gamma}\mathbf{\Lambda}\mathbf{D}_h\mathbf{\Gamma}^{\mathcal{H}}\mathbf{F}\mathbf{u}(i) + \mathbf{\Gamma}\mathbf{F}\tilde{\mathbf{v}}(i), \tag{32}$$

where $\mathbf{\Lambda} = e^{-j\pi\frac{\epsilon(N-1)}{N}}\mathbf{F}\mathbf{D}_f\mathbf{F}^{\mathcal{H}}$ is an $N \times N$ circulant matrix, whose $(m,n)^{\text{th}}$ entry is given by

$$[\mathbf{\Lambda}]_{m,n} = \frac{\sin(\pi((n-m)_N + \epsilon))}{N\sin(\frac{\pi}{N}((n-m)_N + \epsilon))} e^{j\pi\frac{N-1}{N}(n-m)_N}, \tag{33}$$

which is basically the inter-carrier interference (ICI) matrix in OFDM systems impaired by CFO, as shown in [15]. Hence, like in OFDM transmissions, the CFO affects OCDM in three ways: a time variant phase rotation, a time invariant phase rotation, and ICI in the frequency domain. However, unlike in OFDM, the symbols are converted back to the time-domain after equalization. Thus, the impact of the CFO on its performance is still unknown. We assume that the receiver is able to compensate for the phase rotation. Since the phase shift is constant for each symbol, it can be estimated as part of the channel so that $\mathbf{D}_h^{\text{eff}} = e^{\frac{j2\pi\epsilon(iP+L)}{N}} e^{j\pi\frac{\epsilon(N-1)}{N}} \mathbf{D}_h$.

The final version of record is available at http://dx.doi.org/10.1109/TWC.2021.3055070

Thus, the equalizer will implicitly compensate for the phase shift introduced by the CFO leading to time-invariant decision regions. With this in mind, Eq. (32) can be simplified as

$$\tilde{\mathbf{s}} = \mathbf{\Gamma\Lambda D}_h\mathbf{\Gamma}^{\mathcal{H}}\mathbf{Fu} + \mathbf{\Gamma F}\tilde{\mathbf{v}}, \tag{34}$$

where each block is independent and thus, the block index has been removed.

Equalizing using an LE, represented by $\mathbf{G}$, and converting to the time-domain results in

$$\hat{\mathbf{u}} = \mathbf{F}^{\mathcal{H}}\mathbf{G\Gamma\Lambda D}_h\mathbf{\Gamma}^{\mathcal{H}}\mathbf{Fu} + \mathbf{F}^{\mathcal{H}}\mathbf{G\Gamma F}\tilde{\mathbf{v}}. \tag{35}$$

In order to analyze the BER performance of OCDM in the presence of CFO, we resort to the SINR at the output of the equalizer $\bar{\gamma}$, whose relationship to the BER is shown in Eq. (22). In fact, from [25], the SINR on the l^{th} channel can be approximated by $\bar{\gamma}(l) \approx \frac{E_s}{\sigma^2(l)}$. The error vector for a block is given by

$$\mathbf{e} = \hat{\mathbf{u}} - \mathbf{u} = \mathbf{F}^{\mathcal{H}}(\mathbf{G\Gamma\Lambda D}_h\mathbf{\Gamma}^{\mathcal{H}} - \mathbf{I})\mathbf{Fu} + \mathbf{F}^{\mathcal{H}}\mathbf{G\Gamma F}\tilde{\mathbf{v}}. \tag{36}$$

When considering ZF equalization, the l^{th} element of the error vector is given by

$$\begin{aligned} e(l) =& \frac{1}{N}\sum_{k=0}^{N-1}\left(\frac{1}{H(k)}e^{-j\frac{\pi}{N}k^2}\sum_{i=0}^{N-1}[\mathbf{\Lambda}]_{k,i}H(i)e^{j\frac{\pi}{N}i^2} - 1\right) \\ &\times \sum_{n=0}^{N-1}u(n)e^{-j\frac{2\pi}{N}ni}e^{j\frac{2\pi}{N}kl} \\ &+ \frac{1}{N}\sum_{k=0}^{N-1}\frac{1}{H(k)}e^{-j\frac{\pi}{N}k^2}\sum_{n=0}^{N-1}\tilde{v}(n)e^{-j\frac{2\pi}{N}k(n-l)}. \end{aligned}$$

Assuming that $\mathbf{u}$ and $\tilde{\mathbf{v}}$ contain i.i.d. samples and are independent of each other, the MSE is given by

$$\begin{aligned} \sigma^2(l) =& E_s\left(\frac{1}{N}\sum_k\left|\frac{1}{H(k)}\sum_i [\mathbf{\Lambda}]_{k,i}H(i)e^{j\frac{\pi}{N}i^2} - 1\right|^2\right. \\ &\left. + \frac{1}{N\gamma}\sum_k\left|\frac{1}{H(k)}\right|^2\right). \end{aligned} \tag{37}$$

Eq. (37) shows that the MSE is affected by the noise, which decreases as γ increases, and interference, which remains constant. This implies the presence of an error floor at high SNR, caused by the interference.

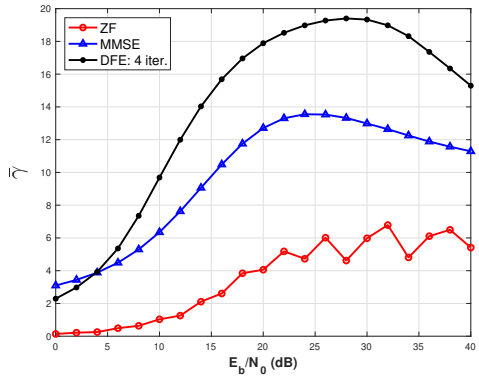

Fig. 9. SINR at the output of the equalizer versus signal SNR for OCDM in the presence of CFO with $\epsilon = 0.1$.

Substituting the values of the MMSE equalizer taps in Eq. (36), we see that the l^{th} element of the vector $\mathbf{e}$ is given by

$$\begin{aligned} e(l) =& \frac{1}{N}\sum_{k=0}^{N-1}\left(\frac{H(k)^\star}{|H(k)|^2 + 1/\gamma}e^{-j\frac{\pi}{N}k^2}\sum_{i=0}^{N-1}[\mathbf{\Lambda}]_{k,i}H(i)e^{j\frac{\pi}{N}i^2} - 1\right) \\ &\times \sum_{n=0}^{N-1}u(n)e^{-j\frac{2\pi}{N}ni}e^{j\frac{2\pi}{N}kl} + \frac{1}{N}\sum_{k=0}^{N-1}\frac{H(k)^\star}{|H(k)|^2 + 1/\gamma}e^{-j\frac{\pi}{N}k^2} \\ &\times \sum_{n=0}^{N-1}\tilde{v}(n)e^{-j\frac{2\pi}{N}k(n-l)}. \end{aligned}$$

Again, utilizing the independence of the noise and symbol vectors, the MSE can be computed as shown in Eq. (38), where a is the element on the main diagonal of $\mathbf{\Lambda}$, i.e., $a = [\mathbf{\Lambda}]_{k,k}$, $k \in [0, N-1]$. Note that as γ increases, so does the magnitude of the term $\mathbb{I}$, whereas the contribution of the noise to the MSE decreases. Beyond a certain SNR, the contribution of the noise becomes negligible but MSE still increases along with SNR. This implies that the output SINR and hence, the BER will start to deteriorate beyond a certain input SNR. Fig. 9 confirms this by numerically computing $\bar{\gamma}$ using simulations. Looking at the curve for ZF equalization, we see that $\bar{\gamma}$ starts to plateau at an input SNR of 20 dB. On the other hand, MMSE and IB-DFE show much higher output SINR than ZF which increases until the input SNR is 20 dB. At this point, the interference starts to dominate and the performance starts to deteriorate as the SNR increases further. This was predicted in Eq. (38). The interference causes error propagation in IB-DFE, thus resulting in a similar trend to that seen for MMSE.

$$\begin{aligned} \sigma^2(l) &= \frac{E_s}{N}\left(\sum_k\left|\frac{H(k)^\star}{(|H(k)|^2 + 1/\gamma)}e^{-j\frac{\pi}{N}k^2}\sum_i[\mathbf{\Lambda}]_{k,i}H(i)e^{j\frac{\pi}{N}i^2} - 1\right|^2 + \frac{1}{\gamma}\sum_k\frac{|H(k)|^2}{(|H(k)|^2 + 1/\gamma)^2}\right) \\ &= \frac{E_s}{N}\left(\sum_k\left|\underbrace{\frac{a|H(k)|^2}{(|H(k)|^2 + 1/\gamma)} + \frac{H(k)^\star}{(|H(k)|^2 + 1/\gamma)}e^{-j\frac{\pi}{N}k^2}\sum_{i\neq k}[\mathbf{\Lambda}]_{k,i}H(i)e^{j\frac{\pi}{N}i^2}}_{\mathbb{I}} - 1\right|^2 + \frac{1}{\gamma}\sum_k\frac{|H(k)|^2}{(|H(k)|^2 + 1/\gamma)^2}\right) \end{aligned} \tag{38}$$

The final version of record is available at http://dx.doi.org/10.1109/TWC.2021.3055070

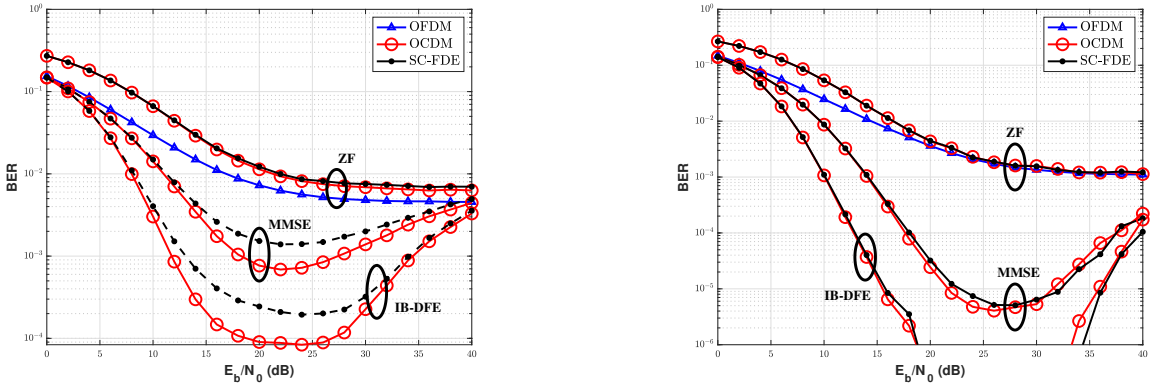

(a) (b)

Fig. 10. Performance comparison of the considered schemes in the presence of CFO with (a) $\epsilon = 0.1$ and (b) $\epsilon = 0.05$.

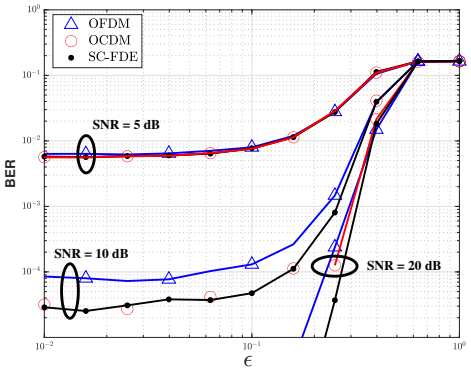

Fig. 11. Performance of coded OCDM in the presence of CFO.

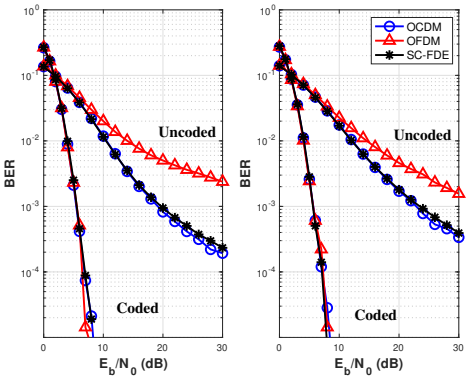

Fig. 12. Performance of OCDM, OFDM and SC-FDE in linear time varying channels with (left) $v = 50$ m/s, and (right) $v = 100$ m/s.

Fig. 10 shows the average uncoded BER for the three transmission formats in the presence of CFO. It can be seen that OCDM and SC-FDE with ZF equalization show approximately the same performance as OFDM with an error floor of approximately 10^{-2} when $\epsilon = 0.1$ and 10^{-3} when $\epsilon = 0.05$. When MMSE or IB-DFE is used, we see that the average BER for OCDM and SC-FDE is significantly lower than OFDM but begins to converge at higher SNRs. IB-DFEs do perform slightly better than MMSE equalization due to their better interference cancellation properties. However, at higher SNR, error propagation starts to dominate leading to performance deterioration. These curves mirror the ones shown in Fig. 9 and confirm the predictions made by Eqs. (37) and (38). A similar trend was observed for SC-FDE systems with channel estimation errors in [25].

Fig. 11 shows the average BER of the three transmission schemes for different ϵ when CC is used. It shows that the performance of all schemes is the same for different operating SNR. When the SNR is larger, the ICI caused by the CFO dominates. However, when the CFO is large, decoding becomes impossible regardless of the operating SNR.

VII. Performance in LTV channels

In LTV channels, equalizing the signal given in Eq. (14) results in the block given by

$$\hat{\mathbf{u}} = \mathbf{G}\mathbf{H}_f\mathbf{\Gamma}^{\mathcal{H}}\mathbf{F}\mathbf{u} + \mathbf{G}\mathbf{F}\tilde{\mathbf{v}}, \tag{39}$$

where $\mathbf{G}$ can be either the ZF or MMSE equalizer defined in Eq. (15) and Eq. (16), respectively.

Fig. 12 compares the performance of the considered schemes in LTV channels for different velocities v with a symbol duration of 1000 μs. The channel is wide-sense stationary with uncorrelated scattering (WSSUS) and there are 9 channel taps with Jakes Doppler spectrum. The figure considers both coded and uncoded performance with a rate-$1/3$ CC being used as the channel code. MMSE equalization is assumed. It can be seen that OCDM and SC-FDE perform identically and show better performance than OFDM for different velocities. This is primarily because uncoded OFDM benfits only from Doppler diversity while OCDM and SC-FDE collects multipath diversity as well. An increase in velocity leads to performance deterioration in OCDM and SC-FDE because of the increase in ICI. As predicted in Section III, OCDM and SC-FDE exhibit identical performance when there is no channel coding. However, when channel coding

The final version of record is available at http://dx.doi.org/10.1109/TWC.2021.3055070

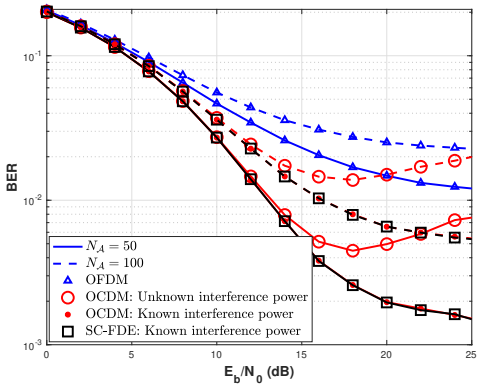

(a) Uncoded

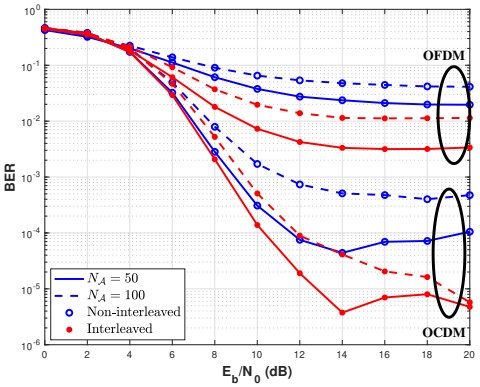

(b) Coded

Fig. 13. BER performance of OCDM in multipath channels with NBI.

is considered, all three schemes show the same performance as coded OFDM can collect multipath diversity as well as Doppler diversity.

VIII. Performance with burst interference

In this section, we compare the performance of OFDM, OCDM, and SC-FDE in the presence of burst interference. Burst interference in the frequency and time domains are referred to as NBI and TBI, respectively.

A. Narrow band interference

We model the n^{th} sample of the i^{th} NBI signal as (c.f., [28])

$$z_i(n) = \sqrt{\frac{E_I}{N}} e^{j\left(\frac{2\pi}{N}(m_i+\alpha)n+\theta_i\right)}, \quad 0 \le n < N + N_g - 1 \tag{40}$$

where E_I is the energy of the interfering symbol, N is the total number of subcarriers, m is the subcarrier closest to the interfering frequency, α is the position of the interference between frequency bins and θ_i is a uniform random variable such that $\theta_i \in [-\pi, \pi)$. For the remainder of this section we assume $\alpha = 0$, that is, the i^{th} interfering signal impacts only the subcarrier given by m_i. We define $\mathcal{A} = \{i : m_i \in [0, N-1]\}$ as the set of active interferer indices and denote its cardinality as $|\mathcal{A}| = N_{\mathcal{A}}$. Hence, it follows that the interfering signal is given by the vector $\mathbf{z} = [\sum_{i\in\mathcal{A}} z_i(0), \sum_{i\in\mathcal{A}} z_i(1), ..., \sum_{i\in\mathcal{A}} z_i(N+N_{\text{g}}-1)]^T$. The received signal is given by

$$\hat{\mathbf{u}} = \mathbf{F}^{\mathcal{H}}\mathbf{G}\mathbf{D}_h\mathbf{F}\mathbf{u} + \mathbf{F}^{\mathcal{H}}\mathbf{G}\mathbf{\Gamma}(\tilde{\mathbf{v}} + \mathbf{z}). \tag{41}$$

We rely on simulations to investigate the performance of OCDM in the presence of NBI. We assume that $N = 2048$ with only 1200 active sub-channels for both OCDM and OFDM and the channel follows the EVA model with tap variances listed in Table I. We simulate both the uncoded and coded cases, employing CC with and without block interleaving and MMSE equalization.

Fig. 13(a) compares the average BER of uncoded OFDM and OCDM with different interfering signal bandwidths. It can be seen that OCDM shows greater resilience to interference in the SNR range of 10–20 dB, beyond which its performance starts to deteriorate. This trend is similar to the one shown by OCDM in the presence of CFO, and is a result of the MMSE equalizer amplifying interference at higher SNRs. In order to account for this, the interfering signal statistics can be incorporated into the MMSE equalizer. Assuming the interference and transmitted signal is independent, the resulting equalizer is given by

$$\mathbf{G} = \text{diag}\left(\frac{H^{\star}(k)}{|H(k)|^2 + (P_{\epsilon} + \mathcal{N}_0)/E_s}\right), \; k \in [0, N-1], \tag{42}$$

where P_{ϵ} denotes the interference energy. Fig. 10(a) shows that when P_{ϵ} is known, the BER no longer deteriorates at higher SNRs but rather exhibits an error floor. Equipped with the knowledge of the interference power, OCDM is considerably more robust to interference than OFDM and depicts a lower error floor. For example, at SNR of 25 dB, OCDM exhibits an approximate BER of 10^{-3}, which is an order for magnitude lower than that of OFDM when $N_{\mathcal{A}} = 50$. The average BER of SC-FDE employing the equalizer shown in Eq. (42) is identical to that of OCDM with the same equalizer.

The comparison of the average BER for coded OCDM and OFDM is shown in Fig. 13(b). In this simulation, we employ CC with a constraint length 7 and rate-1/3 and assume the equalizer is the one given by Eq. (42). In the interleaved case, the bits are interleaved using a block interleaver. Coded OFDM without interleaving shows no improvement over uncoded OFDM because the bits on the subcarriers that experience interference are lost completely and the code cannot correct for this. However, in OCDM the interference is spread out evenly over all the symbols and its impact is mitigated as a result. This allows for accurate decoding at the receiver and channel coding shows significant improvement over uncoded OCDM. For example, at an SNR of 20 dB, uncoded OCDM exhibits an average BER of 2×10^{-3} when $N_{\mathcal{A}} = 50$. Coding decreases BER to 10^{-4} and interleaving enhances it further to 7×10^{-6}. Interleaving also enhances the performance of OFDM by an order of magnitude as well. However, OCDM still performs significantly better than OFDM. Symbol interleaving can be used to further enhance OFDM performance at the cost of delay but such schemes will not be discussed as they are

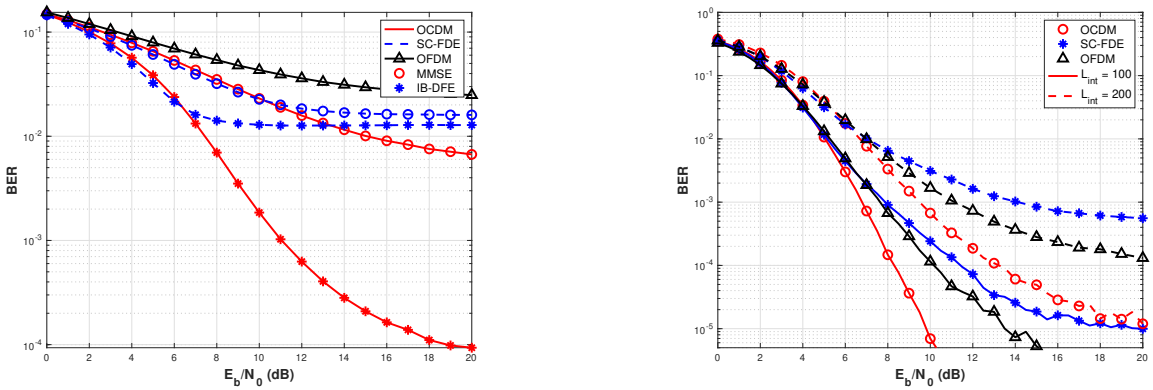

(a) Uncoded (b) Coded

Fig. 14. Performance comparison in the presence of TBI. $L_{\text{int}} = 100$ for (a). For (b), a rate 1/3 CC is used.

beyond the scope of this work. Since uncoded SC-FDE shows the same error performance as OCDM, it follows that this will extend to coded comparisons. Hence, in the interest of brevity, it has been omitted.

B. Time burst interference

Having seen that OCDM is more robust to NBI than OFDM owing to the fact that each symbol is spread in the frequency domain, we now compare the performance of the three schemes when the interference is constrained in time. Thus, the length$-N$ interfering signal block is defined as

$$z(n) = \begin{cases} a_n & \text{if } \frac{N-L_{\text{int}}}{2} \leq n < \frac{N+L_{\text{int}}}{2}, \\ 0 & \text{otherwise}, \end{cases} \tag{43}$$

where a_n are i.i.d. complex symbols drawn from the QPSK alphabet such that $\mathbb{E}[|a_n|^2] = E_s$ and $L_{\text{int}} < N$ is the length of the TBI. Note that the interfering signal is always positioned in the center of the signal of interest so that removing the CP has no impact on the TBI.

Fig. 14 compares the performance of the three schemes in the presence of TBI with and without channel coding. We assume the equalizers incorporate knowledge of the interference strength. For MMSE, this corresponds to the equalizer defined in Eq. (42). In IB-DFE, the feed-forward filter coefficients are modified, as shown in [25]. The underlying channel is assumed to be LTI. The uncoded performance of OCDM is considerably better than both other schemes as shown in Fig. 14(a). SC-FDE mainly suffers because the symbols that experience interference become undetectable but in OCDM, the interference is spread out evenly. Although this is also the case for OFDM, its performance suffers because of lower SNR on each subcarrier and because independent detection causes the worst performing subcarrier to dominate. Fig. 14(b) shows the performance of each scheme with channel coding. We assume DFE for OCDM and SC-FDE and MMSE equalization for OFDM. Although channel coding is able to improve the error rate for all three transmission schemes, SC-FDE still performs worse as coding is not able to sufficiently compensate for burst errors. Both OFDM and OCDM perform better because the interference is spread over the entire symbol. However, OCDM still shows considerably better performance. Increasing L_{int} leads to performance deterioration for all three schemes. In OCDM, this occurs because the SINR is a function of L_{int}. This also implies that increasing the interference energy will similarly impact the SINR and lead to performance deterioration for OCDM. Thus, it can be concluded that the performance of OCDM is conditioned on the energy of the interfering signal and its duration. More persistent interference and higher interference energy may cause OCDM and SC-FDE to start exhibiting similar performance.

IX. Conclusion

This paper thoroughly analyzed the performance of OCDM for wireless channels with and without synchronization errors and interference. The results showed uncoded OCDM performs significantly better than uncoded OFDM in both LTI and LTV channels because of its ability to collect multipath diversity. However, due to the similarities in the transmission formats, SC-FDE and OCDM have identical performances. When channel coding is employed, the performances of all three schemes start to converge mainly because OFDM benefits much more from channel codes than OCDM or SC-FDE. In the presence of CFO, the results exhibited an interesting trend for OCDM and SC-FDE transmissions when the IB-DFE or MMSE equalizers were used. It was shown that due to interference enhancement and error propagation, the BER for uncoded OCDM and SC-FDE degrades at higher SNRs. However, at moderate SNR, OCDM and SC-FDE were demonstrated to be more resilient to the interference caused by CFOs than OFDM. This changed when channel coding was employed as coded OFDM showed the same BER performance as coded OCDM and SC-FDE. A similar trend of interference enhancement was also shown for OCDM in the presence of NBI. However, by incorporating knowledge of the interference energy in the MMSE and IB-DFE equalization, OCDM was shown to have significantly better performance than OFDM in the presence of both NBI and TBI. Because OCDM spreads symbols in both the time and frequency domains, it also showed considerably better performance than SC-FDE when TBI was considered. Lastly, the study showed that OCDM

suffers from the same high PAPR as OFDM, a problem that does not occur in SC-FDE.

This work, however, is in no way comprehensive and much remains to be done. In the near future, we will further investigate modulation and detection schemes for OCDM e.g., differential detection, and its performance in the presence of fast fading channels. Channel estimation techniques also need to be devised for OCDM, particularly those involving comb and lattice structured pilots to better estimate time varying channels.

REFERENCES

[1] A. Osseiran et al., "Scenarios for 5G mobile and wireless communications: the vision of the METIS project," *IEEE Commun. Mag.*, vol. 52, no. 5, pp. 26-35, May 2014.
[2] X. Ouyang and J. Zhao, "Orthogonal chirp division multiplexing," *IEEE Trans. Commun.*, vol. 64, no. 9, pp. 3946-3957, Sept. 2016.
[3] X. Ouyang and J. Zhao, "Orthogonal chirp division multiplexing for coherent optical fiber communications," *J. Lightw. Technol.*, vol. 34, no. 18, pp. 4376-4386, Sept.15, 2016.
[4] X. Ouyang, G. Talli, M. Power and P. Townsend, "Orthogonal chirp-division multiplexing for IM/DD-based short-reach systems," *Opt. Express,* 2019.
[5] X. Ouyang, C. Antony, G. Talli and P. D. Townsend, "Robust channel estimation for coherent optical orthogonal chirp-division Multiplexing With pulse compression and noise rejection," *J. Lightw. Technol.,* vol. 36, no. 23, pp. 5600-5610, Dec.1, 2018.
[6] R. Bomfin, M. Chafii and G. Fettweis, "Performance assessment of orthogonal chirp division multiplexing in MIMO space time coding," in *Proc. IEEE 2nd 5G World Forum (5GWF),* Dresden, Germany, 2019.
[7] M. S. Omar and X. Ma, "Designing OCDM-based multi-user transmissions," in *Proc. IEEE Global Commun. Conf. (GLOBECOM),* Waikoloa, HI, USA, 2019, pp. 1-6.
[8] M. S. Omar and X. Ma, "Spectrum design for orthogonal chirp division multiplexing transmissions," *IEEE Wireless Commun. Lett.,* vol. 9, no. 11, pp. 1990-1994, Nov. 2020.
[9] X. Ouyang, O. A. Dobre, Y. L. Guan, and J. Zhao, "Chirp spread spectrum toward the Nyquist signaling rate–orthogonality condition and applications," *IEEE Signal Process. Lett.,* vol. 24, no. 10, pp. 1488-1492, Oct. 2017.
[10] P. J. Bouvet, Y. Auffret, and C. Aubry, "On the analysis of orthogonal chirp division multiplexing for shallow water underwater acoustic communication," in *Proc. OCEANS*, Aberdeen, 2017, pp. 1-5.
[11] P. Zhu, X. Xu, X. Tu, Y. Chen and Y. Tao, "Anti-Multipath orthogonal chirp division multiplexing for underwater acoustic communication," *IEEE Access,* vol. 8, pp. 13305-13314, 2020.
[12] L. de M. B. A. Dib, G. R. Colen, M. de L. Filomeno and M. V. Ribeiro, "Orthogonal chirp division multiplexing for baseband data communication systems," *IEEE Syst. J.,* vol. 14, no. 2, pp. 2164-2174, June 2020.
[13] R. Bomfin, M. Chafii and G. Fettweis, "Low-Complexity Iterative Receiver for Orthogonal Chirp Division Multiplexing," in *IEEE Wireless Commun. and Netw. Conf. (WCNC)* Marrakech, Morocco, 2019, pp. 1-6, doi: 10.1109/WCNCW.2019.8902857.
[14] X. Ma, C. Tepedelenlioglu, G. B. Giannakis, and S. Barbarossa, "Non-data-aided carrier offset estimators for OFDM with null subcarriers: identifiability, algorithms, and performance," *IEEE J. Sel. Areas Commun.,* vol. 19, no. 12, pp. 2504-2515, Dec. 2001.
[15] L. Rugini and P. Banelli, "BER of OFDM systems impaired by carrier frequency offset in multipath fading channels," *IEEE Trans. Wireless Commun.,* vol. 4, no. 5, pp. 2279-2288, Sept. 2005.
[16] M. Ghogho, V. P. Gil-Jimenez, and A. Swami, "Multipath diversity and coding gains of cyclic-prefixed single carrier systems," in *Proc. Int. Conf. Acoustics, Speech and Signal Processing*, Taipei, 2009, pp. 2837-2840.
[17] Z. Liu, Y. Xin, and G. B. Giannakis, "Linear constellation precoding for OFDM with maximum multipath diversity and coding gains," *IEEE Trans. Commun.*, vol. 51, no. 3, pp. 416-427, Mar. 2003.
[18] Z. Wang and G. B. Giannakis, "A simple and general parameterization quantifying performance in fading channels," *IEEE Trans. Commun.,* vol. 51, no. 8, pp. 1389–1398, Aug. 2003.
[19] Y. Lin and S. Phoong, "BER minimized OFDM systems with channel independent precoders," *IEEE Trans. Sig. Proc.,* vol. 51, no. 9, pp. 2369-2380, Sept. 2003.
[20] Y. Lin and S. Phoong, "MMSE OFDM and prefixed single carrier systems: BER analysis," in *Proc. IEEE Int. Conf. Acoust., Speech, Sig. Process.,* Hong Kong, 2003, pp. 229–232.
[21] Y. Lin and S. Phoong, "BER optimized channel independent precoder for OFDM system," in *Proc. IEEE Global Telecommun. Conf.,* Taipei, Taiwan, 2002, pp. 350–354 vol. 1.
[22] 3GPP TS 36.101. "Evolved Universal Terrestrial Radio Access (E-UTRA); User Equipment (UE) Radio Transmission and Reception." *3rd Generation Partnership Project; Technical Specification Group Radio Access Network.* URL: https://www.3gpp.org.
[23] D. Wulich, N. Dinur, and A. Glinowiecki, "Level clipped high-order OFDM," *IEEE Trans. Commun.,* vol. 48, no. 6, pp. 928-930, Jun. 2000.
[24] T. Pollet, M. Van Bladel, and M. Moeneclaey, "BER sensitivity of OFDM systems to carrier frequency offset and Wiener phase noise," *IEEE Trans. Commun.,* vol. 43, no. 2/3/4, pp. 191-193, Feb/Mar/Apr., 1995.
[25] N. Souto, R. Dinis, and J. C. Silva, "Impact of channel estimation errors on SC-FDE systems," *IEEE Trans. Commun.*, vol. 62, no. 5, pp. 1530-1540, May 2014.
[26] N. Benvenuto and S. Tomasin, "Iterative design and detection of a DFE in the frequency domain," in *IEEE Trans. Commun.,* vol. 53, no. 11, pp. 1867-1875, Nov. 2005.
[27] R. Dinis, P. Montezuma, N. Souto and J. Silva, "Iterative frequency-domain equalization for general constellations," in *IEEE Sarnoff Symp.,* Princeton, NJ, 2010, pp. 1-5.
[28] A. Batra and J. R. Zeidler, "Narrowband interference mitigation in OFDM systems," in *Proc. IEEE Military Commun. Conf.,* San Diego, CA, 2008, pp. 1-7.
[29] M. S. Omar and X. Ma, "The effects of narrowband interference on OCDM," in *Proc. IEEE 21st Int. Workshop Sig. Process. Adv. in Wireless Commun. (SPAWC),* Atlanta, GA, USA, 2020.

Muhammad Shahmeer Omar received the B.S. degree in Electrical Engineering from the National University of Sciences and Technology (NUST), Pakistan in 2015 and the M.S. degree in Electrical and Computer Engineering from Georgia Tech, USA in 2018 where he is currently pursuing a Ph. D. His research interests include multicarrier transmission technologies, signal processing and machine learning for communications, and diversity techniques for fading channels.

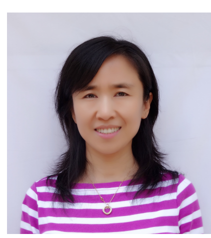

Xiaoli Ma (F'16) received the B.S. degree in Automatic Control from Tsinghua University, Beijing, China in 1998, the M.S. degree in Electrical Engineering from the University of Virginia in 2000, and the Ph.D. degree in Electrical Engineering from the University of Minnesota in 2003. After receiving her Ph.D., Dr. Ma joined the Department of Electrical and Computer Engineering at Auburn University, where she served as an assistant professor until Dec. 2005. Since Jan. 2006, she has been with the School of Electrical and Computer Engineering at Georgia Tech, where she is currently a professor. She was awarded the Lockheed Martin Aeronautics Company Dean's Award for Teaching Excellence by the College of Engineering in 2009, and Outstanding Junior Faculty Award by the School of Electrical and Computer Engineering in 2010, at Georgia Tech. Her research focuses on wireless networking and communications, including network performance analysis, transceiver designs for wireless time- and frequency-selective channels, channel estimation and equalization algorithms, carrier frequency synchronization for OFDM systems, Internet of Things, and performance analysis for blockchains. Dr. Ma served as a Senior Area Editor for *IEEE Signal Processing Letters* (2014-2017) and *Elsevier Digital Signal Processing* (2012 - 2016), and has been an Associate Editor for *IEEE Signal Processing Letters* (2007-2009) and *IEEE Transactions on Wireless Communications (2008-2013)*. She was a co-director for Gatech Center of Excellence on UWB Technology.